Train Vibrations Reveal Internal Changes in a High-Speed Railway Viaduct System through Dispersion-Change Patterns of a Fast Guided Wave

Yongxiang Shi[1], Jingchong Wen[2], Han Wu[3], Mingjia Li[4], Zhichao Yu[1], Chuan He[2], Ling Chen[1]*, and Jieyuan Ning[2]

[1]State Key Laboratory of Lithospheric and Environmental Coevolution, Institute of Geology and Geophysics, Chinese Academy of Sciences, Beijing 100029, China

[2]School of Earth and Space Sciences, Peking University, Beijing 100871, China

[3]Institute of Geophysics, China Earthquake Administration, Beijing 100081, China

[4]Department of Earth and Space Sciences, Southern University of Science and Technology, Shenzhen 518055, China

Key points

- Using passing trains, we identify a fast guided wave in a high-speed railway viaduct system and track its dispersion curve hourly
- Within 28 days we find two dispersion-change patterns: a diurnal cycle of up to 4% that reverses near 7 Hz and a 0.6% multi-day offset
- The two patterns follow air temperature and groundwater level and reflect changes in different parameters of the viaduct system

Abstract

High-speed trains generate highly repeatable seismic vibrations, whose changes are expected to reveal how railway infrastructure changes over time. From a dense array and 28 days of trains, we use seismic interferometry to extract a fast guided wave along the viaduct hour by hour. The wave travels at about 3000 m/s with a single S-shaped branch, and its dispersion has two change patterns: a diurnal cycle of up to 4% that reverses near 7 Hz, and a 0.6% multi-day change. Fitting attributes the diurnal cycle to the resonance frequency and the coupling parameter, both tracking air temperature. The multi-day change can come from the waveguide velocity and coincides with an irrigation-driven groundwater fall. Together, these observations indicate that the viaduct system is locally resonant, and the frequency pattern identifies which internal parameter of the system has changed. This offers a new seismological means for monitoring railway bridge health.

Plain Language Summary

High-speed rail runs largely on bridges, but the internal state of a viaduct and its foundations is hard to monitor. Our study finds that the vibrations of passing trains can help detect internal changes in an HSR viaduct system. We placed a dense line of sensors along an HSR viaduct and recorded 28 days of trains. By comparing the vibrations at different sensors, we extracted a wave that travels along the viaduct at about 3 km/s, and we tracked, hour by hour, how its speed varies with frequency. The speed changes in two ways: a daily cycle of up to 4% that follows the air temperature, and a slower change of about 0.6% over several days that coincides with a fall of the groundwater level. Because the two changes appear at different frequencies, they reveal which part of the viaduct system is changing. The method uses only the trains that pass anyway, and it can be extended to the more than 20,000 km of HSR bridges, offering a new perspective on bridge health monitoring.

1 Introduction

High-speed rail (HSR) is a transport system that has been built and is still expanding worldwide; in China alone it has grown to 50,000 km (National Railway Administration, 2026). To operate and maintain this vast network over the long term, health monitoring of its infrastructure is essential, and sensing approaches are being developed for this purpose (Fu et al., 2026; G. Wang et al., 2025; Hao et al., 2025). Notably, trains gen-

erate strong seismic vibrations, and hundreds of train events a day form a highly repeatable source sequence along the line (Brenguier et al., 2019; Y. Liu et al., 2021b). Monitoring the changes of these vibrations and clarifying their internal mechanisms is therefore expected to provide a new seismology-based perspective for railway infrastructure health monitoring.

Train sources are deterministic in space, time and frequency spectrum, with positions fixed by the track and spectra by train speed and formation, yet their phase is unpredictable, as for a passive source (X. Wang et al., 2019; Wen et al., 2021; Y. Liu et al., 2021b, 2021a; Jiang et al., 2022; X. Wang et al., 2026). For such a deterministic passive source, seismic interferometry (Schuster, 2009) makes full use of this determinacy to extract ballistic-wave signals along the line from a small number of events, including typical Rayleigh waves and guided P waves (Mi & Xia, 2023, 2026; Shao et al., 2022; Yin et al., 2024; Y. Zhang et al., 2019). Monitoring based on such ballistic waves can therefore identify the specific origin of the changes (Brenguier et al., 2019, 2020; Sheng et al., 2022; Mukherjee et al., 2026; Cheng et al., 2025).

On an HSR line, however, the structure itself complicates this task, because the 50,000-km network in China is built largely on viaducts, with more than 10,000 bridges totalling more than 20,000 km in length (L. Chen & Yan, 2022; National Railway Administration, 2026). These periodic structures, through their collective behavior, make the wavefield far more complex than on an ordinary line (He et al., 2017). Previous studies show that periodic piers produce strong crosstalk and stacking, Doppler effects in the wavefield, and source radiation patterns that are directional and frequency-selective (Jiang et al., 2022; Shi et al., 2022; Wen et al., 2021; X. Wang et al., 2026). Moreover, although each pier is much smaller than the wavelength, the numerous periodic subwavelength structures can still modulate the wavefield, as in locally resonant metamaterials (Z. Liu et al., 2000; Colombi et al., 2016; Fang et al., 2006).

For such a multi-component complex wavefield, how to monitor its internal changes and identify their causes remains an open question. Here we propose that a possible solution lies in monitoring the dispersion-change pattern of a fast guided wave along HSR. We deployed a dense array beneath the HSR viaduct and used passing trains as the source to extract a fast guided wave that travels along the viaduct. Over 28 days of observation, we resolve two patterns of dispersion change in this wave. The shape of the disper-

sion curve and the two change patterns both point to a locally resonant system formed by the viaduct along the line, while the system components and their coupling are driven by different physical factors. This means that the dispersion-change pattern can identify which part of this locally resonant bridge system has changed, providing a new technical path for health monitoring of the more than 20,000 km of HSR bridges.

2 Data and Methods

The data come from a dense array deployed in June 2024 along the Beijing–Guangzhou HSR (Figures 1a and 1b). The array was deployed beneath a typical viaduct more than 10 km long, with a station spacing of about 32 m. The observation began on 30 May 2024 and lasted about four weeks, continuously recording more than 8000 train events. The Beijing–Guangzhou HSR is one of the busiest lines in China, with nearly 300 train events per day. We selected a 3-km segment with 90 stations and 6641 events for stacking and monitoring (Figure S1). Within the 40-s window for interferometry, the train is always north of the array, which keeps the source azimuth fixed and avoids acausal crosstalk (Figure 1b). We then applied phase-only spectral whitening and stacked the results to obtain virtual shot gathers, with station P280 as the virtual source (Figure 1c,and Text S1).

In the virtual shot gathers along the viaduct, we observe a fast guided wave generated by the train (Figures 1c and 1e). The wave is the dominant component above 4 Hz, with clear dispersion and phase velocities of the order of 3000 m/s, and a turning point near 7 Hz. It keeps this high velocity up to about 30 Hz (Figure S2), far above the shallow V_S profile, which is below 800 m/s in the top 140 m (Figures S3, S4). Between 5 and 30 Hz, we observe no coexisting higher-order branches. Meanwhile, in both train-source and ambient-noise interferometry (Figures S2, S3), the wave has the same dispersion pattern, with weak energy near 7 Hz in both. We use the dominant wave for the subsequent velocity monitoring.

Then we stack events hour by hour into virtual shot gathers to monitor the temporal variation of the guided-wave dispersion curve (Figures 1d, 1f). We find one-hour stacking of about 13 train events gives clear guided-wave signals (Figures S5, S6). As shown in Figure 1d, the signal at the same station pair remains highly consistent in time, providing the basis for extracting these changes. We then taper the signal and apply a

frequency–velocity (FV) transform along the array (Figure S5). At each frequency, taking the maximum in the FV domain gives the phase velocity for that time window (Figure 1f), and hence the full dispersion curve of the window (Figure S6). Time resolution is the key metric for monitoring (Clarke et al., 2011), and we find that a 1-hour stack already resolves the phase-velocity change clearly at 6.5 Hz (Figure 1f), while over a wider band, such as 5–11 Hz, the effective resolution is between 1 and 3 hours (Figures S5, S6).

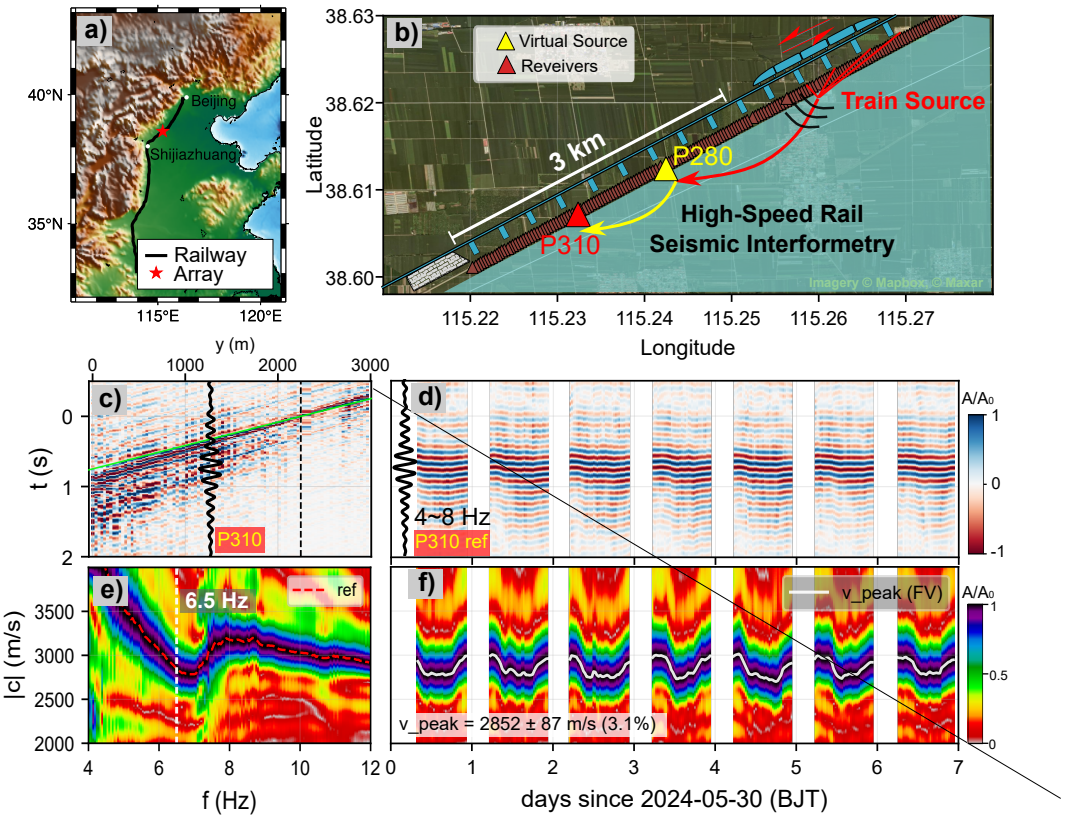


Figure 1. Observation system and extraction of the dispersion change. (a) Location of the observation system, on the Beijing–Shijiazhuang section of the Beijing–Guangzhou HSR; the array lies beneath a viaduct more than 10 km long. (b) Geometry of the array and the seismic interferometry along the viaduct; details in Figure S1. (c) Virtual shot gather obtained by stacking; the virtual source is P280. (d) Signals at station P310 stacked in successive 1-hour windows. (e) FV-domain energy distribution of the virtual shot gather; the red line is the reference dispersion curve of the guided wave. (f) FV slices at 6.5 Hz for successive time windows, with the picked phase velocity in white. The gaps at night in (d) and (f) are train-free periods with too few events.

3 Results

3.1 Diurnal dispersion changes

The velocity of the guided wave shows a clear diurnal cycle (Figure 2a). We take the reference dispersion curve from all events (Figure 1e) as the baseline velocity and convert the hourly phase-velocity shift dv at each frequency into a dimensionless relative change, $dv/v(f,t)$ (Figures 2a, S6). At 6.5 Hz, $dv/v(t)$ shows a clear diurnal cycle over the 28 days, with a mean amplitude of about 4%. Both the cycle and its amplitude vary from day to day; on days 15 and 22 the daily amplitude drops markedly. This variation correlates significantly with the local air temperature (NOAA National Centers for Environmental Information, 2001; Smith et al., 2011), with $R = -0.82$ overall (Figures S7, S8).

The velocity change also varies strongly with frequency (Figures 2b, 2c, 2d). Figure 2b shows $dv/v(f,t)$ across the full dispersion curve, and the two bands separate clearly near 7 Hz. The amplitude $A(f)$ and phase $\phi(f)$ of the diurnal cycle confirm this separation quantitatively (Figures 2c, d). Below 7 Hz, $A(f)$ rises from about 2% to about 4% near 6.8 Hz, while $\phi(f)$ stays essentially constant, so the change is synchronous across the band. Above 7.5 Hz, $A(f)$ recovers to about 4% and then decays with frequency. The two bands differ in phase by about half a cycle (12 h), so that dv/v above 7.5 Hz is opposite in sign to that below 7 Hz.

Notably, the turning point of the dispersion curve and the sign reversal of the velocity change both occur around 7 Hz, where the energy of the virtual shot gathers is also clearly weak (Figures S2, S3). A reasonable conjecture is therefore that these phenomena are different manifestations of the same mechanism. We next introduce a locally resonant model to account for them theoretically.

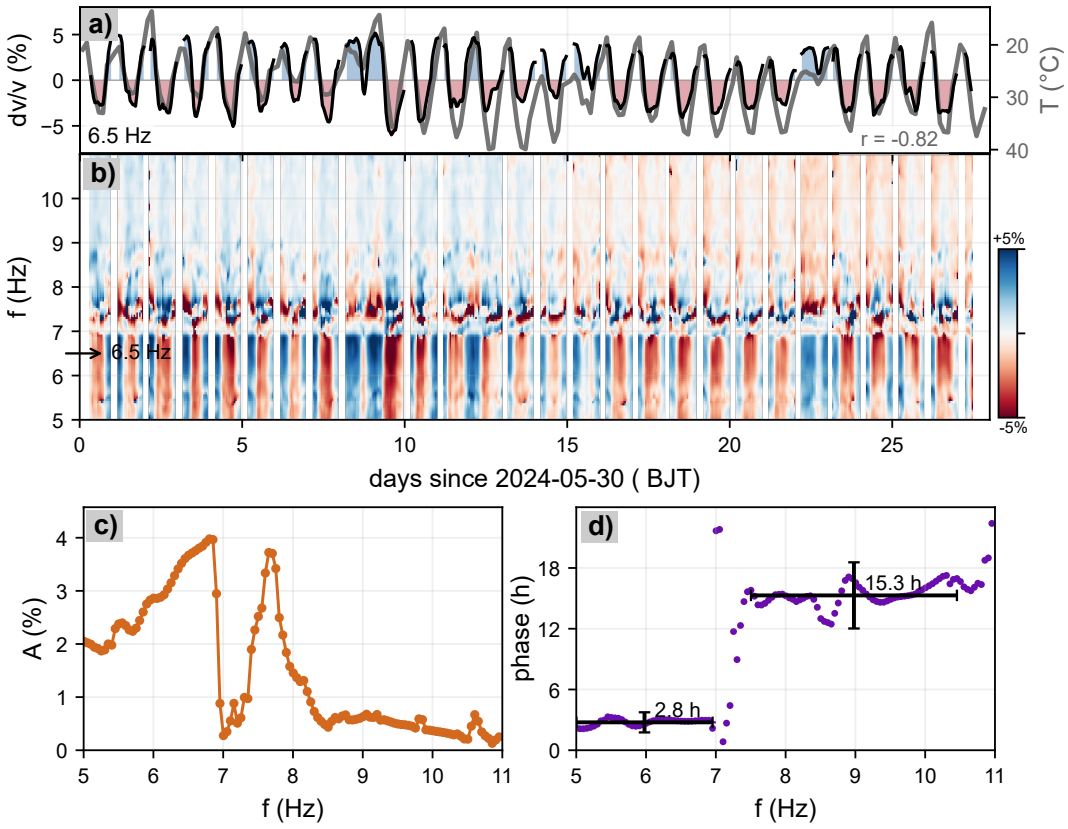


Figure 2. Diurnal variation and frequency dependence of the velocity along the viaduct. (a) Velocity change over 28 days and its correlation with temperature. The black line is the velocity change; blue and red mark the high- and low-velocity periods, respectively. The grey line is air temperature recorded at the local weather station (Figure S7). (b) Distribution of the velocity change at different frequencies; the reference velocity at each frequency is shown in Figure 1e. (c) The amplitude $A(f)$ of the velocity change for the 1 cycle/day component, with the maximum about 4%. (d) Phase $\phi(f)$ of the velocity change for the same period: below 7 Hz the velocity peaks at 2.8 h local time, whereas above 7.5 Hz it reaches a maximum at 15.3 h local time. The overall time resolution is 3 h, which reduces the noise level in the high-frequency band.

3.2 The diurnal change comes from the second resonator

To explain the dispersion of the guided wave and to locate the internal origin of its changes, we simplify the viaduct system into a theoretical model composed of a waveguide loaded with resonators (Figure 3). The waveguide represents the unperturbed primary wavefield that propagates continuously along railway, whose wavelength is much larger than the scale of the structure. The resonators represent the response of the pe-

riodic viaduct structure to this wave. Together the two components form a locally resonant system, in which the resonators induce dispersion of the guided wave near their resonance frequencies and produce a single-branch S-shaped dispersion curve (Z. Liu et al., 2000; Fang et al., 2006; Z. Chen et al., 2022). In a mass-dominated resonant system (Huang et al., 2009), the theoretical phase velocity is (Text S2):

$$c_{\text{eff}}(\omega) = \text{Re}\left[c_0 \Big/ \sqrt{1 + \sum_{j=1,2} \gamma_j \frac{\tilde{\omega}_j^2}{\tilde{\omega}_j^2 - \omega^2}}\right], \tag{1}$$

where c_0 is the intrinsic velocity of the waveguide. j labels the resonators; their complex eigenfrequencies $\tilde{\omega}_j$ ($\tilde{\omega}_j^2 = \omega_j^2 - i\omega_j\omega/Q_j$) are defined by the resonance frequency ω_j and the quality factor Q_j. γ_j is the effective mass ratio of the resonator to the waveguide and measures the coupling strength between them.

Within this framework, a model with two resonators fits the observed dispersion curve well (Figures 3a, S6, S9). A single resonator induces a minimum in the phase velocity just below its resonance frequency and a maximum just above it (Fang et al., 2006). The observed dispersion curve shows a maximum below 5 Hz and another near 8 Hz. The curve therefore results from the joint action of two resonators, at $f_1 \approx 4$ Hz and $f_2 \approx 7$ Hz, with a waveguide velocity c_0 of about 2800 m/s (Figure S9). The first resonance is constrained mainly by the shape of the curve above 5 Hz and is therefore less well determined than the second.

Fitting the dispersion curves (Text S3) shows that the diurnal cycle is dominated by changes in f_2 and γ_2 of the second resonator (Figures 3a, 3b). We divide the events into two subsets according to the sign of dv/v at 6.5 Hz in Figure 2a, and stack them separately, obtaining two clearly different dispersion curves, curve H ($dv/v|_{6.5\,\text{Hz}} > 0$) and curve L ($dv/v|_{6.5\,\text{Hz}} < 0$). The difference between them reverses sign across 7 Hz (Figures 3a, 3b), consistent with the behavior of $A(f)$ and $\phi(f)$ (Figures 2c, 2d). The fits show that the difference between curves H and L comes mainly from a joint change in the frequency f_2 and the coupling coefficient γ_2 of the second resonator, while the remaining parameters, c_0 and others, show no clear change (Figure S9). Relative to curve H, f_2 of curve L decreases by 2.9%, from 7.26 Hz, whereas γ_2 increases by 32%, making the velocity change reverse near the resonance frequency of about 7 Hz.

We apply the same fitting to every dispersion curve measured at each time step (Figure S6) to obtain the time series of f_2 and γ_2 (Figures 3c, S10). The two parameters vary

in opposite phase ($r = -0.80$) and both correlate with the local air temperature (Figures 3d, 3e), with sensitivities of $\partial f_2/\partial T = -0.26\%$ and $\partial \gamma_2/\partial T = +2.3\%$ per °C. Substituting these time series into the model reproduces the observed diurnal change (Figure S11), supporting a resonance-parameter origin for the diurnal cycle.

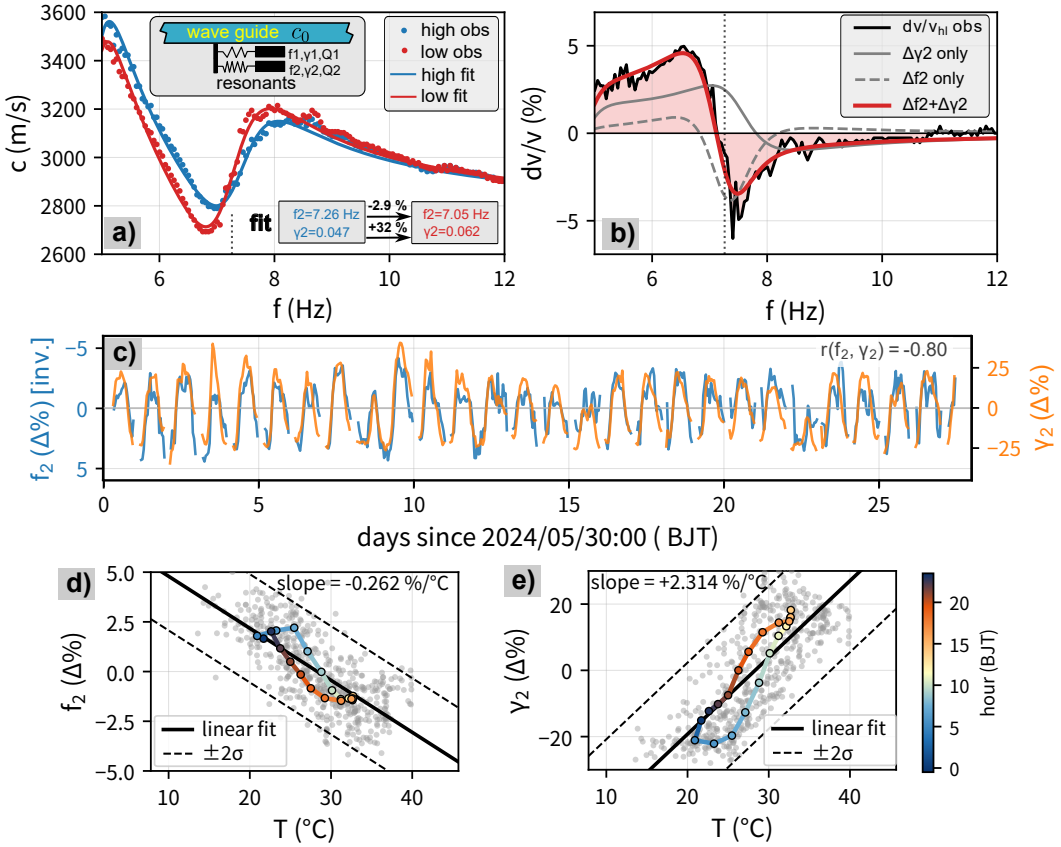


Figure 3. Dispersion pattern and analysis of the diurnal-change origin. (a) The two dispersion curves H and L, in blue and red. The theoretical model of the locally resonant system comprises a waveguide and resonators; solid lines in (a) are the fitted dispersion curves. (b) Relative difference between the two dispersion curves: the black line is the observed dv/v, grey lines are the best fits obtained by changing only γ_2 or only f_2, and the red line is the best fit obtained by changing both. (c) Time series of the fitted parameters for the dispersion curves of all time windows over 28 days; blue is f_2 and orange is γ_2. (d,e) Correlation of the local air temperature with the fitted parameters, f_2 (d) and γ_2 (e); the coloured points mark the hour of the day, so the closed loop traces the daily cycle. Fitting details, parameters and the comparison with the observations are given in Figures S9, S10 and S11.

3.3 A multi-day change in the waveguide velocity

Besides the diurnal change, there is a multi-day change pattern in the viaduct system (Figure 4a). In the raw observations (Figure 2b), $dv/v(f,t)$ is systematically larger before day 15 than after it. This feature becomes clearer after removing the diurnal change produced by f_2 and γ_2 and smoothing over 24 h (Figure 4a). The residual change is nearly uniform in frequency, in contrast to the diurnal pattern.

Stacking the events before day 13 (12 June 2024) and after day 17 (16 June 2024) separately gives two dispersion curves, curve Pre and curve Post (Figure 4c). The difference between the two dispersion curves is an overall offset of about 0.6% (Figure 4d) that extends up to 30 Hz (Figure S12). Within this locally resonant model, only a change in the intrinsic waveguide velocity c_0 enters the effective velocity independently of frequency, so such a broadband, frequency-independent pattern can only be produced by a change in c_0 (Figure S13).

This change took place within a few days and then remained stable. To determine the mechanism of this change, we compared it with the multi-day variation of other factors and found it to be synchronous with the change in groundwater level (Figure 4b). During the period of the c_0 change, the water table around the line, which lies at a depth of 20–30 m, fell by about 1 m, caused by agricultural irrigation during the corn-sowing season in the North China Plain (G. Zhang et al., 2015) (Figure S14). We analysed the daily variation of c_0 (Figure S15) and found it to be more strongly correlated with the groundwater level than with mean air temperature and surface pressure (Figure S16). Between the two we observe a linear quantitative relation over the observed drawdown: a 1-m fall of the water table corresponds to a decrease of about 0.76% in c_0 ($r = +0.98$; Figure 4e).

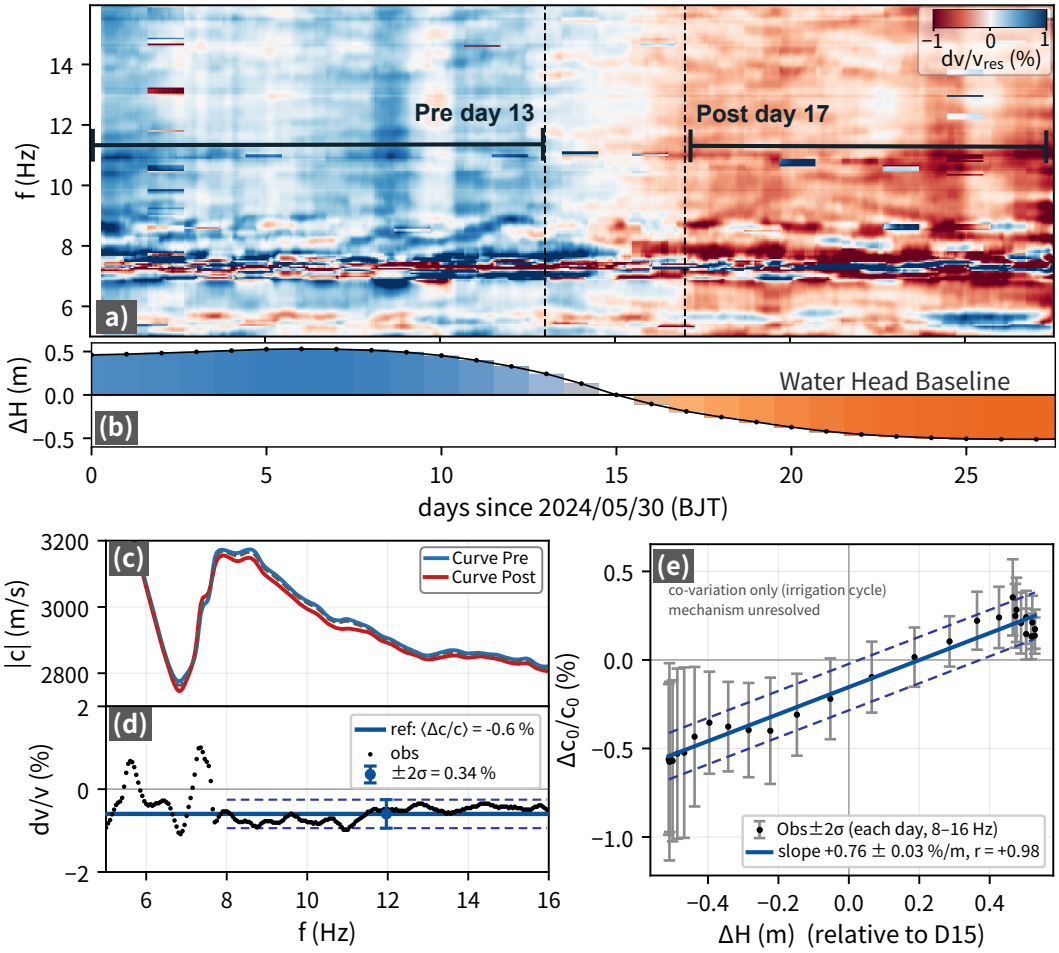


Figure 4. Multi-day change of the guided-wave velocity and its relation to the water level. (a) Residual velocity change $dv/v_{res}(f,t)$ smoothed over 24 h; dashed lines mark the two periods compared below. (b) Change in the four-well median hydraulic head relative to day 15, in blue where the level is higher and orange where it is lower. (c) Dispersion curves obtained by stacking the events of the two periods separately. (d) Observed velocity difference between the two periods (black dots, $\pm 2\sigma$) and the difference predicted by a -0.6% change in c_0 (blue dashed line). (e) Daily $\Delta c_0/c_0$ (band mean over 8–16 Hz) against the water-level change, with $\pm 2\sigma$ error bars.

4 Discussion

Using seismological velocity monitoring, we have revealed how the locally resonant system of the viaduct changes. Understanding the mechanism requires knowing which path the wave propagates within the viaduct system. We therefore discuss two possibilities based on the present observations: a subsurface P wave and an above-ground bridge wave.

In the subsurface hypothesis, the waveguide is a deep P-wave structure, and the resonators may be formed by resonance of the soil between the piers. Along HSR lines, previous studies have shown that seismic interferometry can extract train-generated P waves (Jiang et al., 2022; Mi & Xia, 2023, 2026). In the study area, although the S-wave velocity above 140 m does not exceed 800 m/s (Figure S4), a waveguide of 2800 m/s can still be formed by virtual head waves from greater depths (Bharadwaj et al., 2012; Brenguier et al., 2020). In addition, the periodic pile foundations divide the shallow soft soil into 32-m cells, which can produce the two resonance modes at f_1 ($\lambda \approx 64$ m) and f_2 ($\lambda \approx 32$ m). The observed shallow S-wave velocity of about 300 m/s is compatible with the wavelengths of these modes.

In the bridge-wave hypothesis, the waveguide is the S_0 guided wave in the girder, and the resonators correspond to specific modes of the piers and other components. A one-dimensional continuous beam can carry the fundamental symmetric (S_0) guided wave (Lamb, 1917), which is approximately non-dispersive at long wavelengths. The longitudinal guided-wave velocity of concrete box-girder components is of the order of 3–4 km/s (J. Liu et al., 2025), slightly higher than but of the same order as the observed c_0 (about 2.8 km/s), consistent with the waveguide component of the locally resonant system. The 32-m span forms a natural periodic structure with abundant structural resonance frequencies, giving rise to a locally resonant system. In this case, f_2 may be related to the transverse swaying mode of the piers, and γ_2 to the coupling strength between the girder and these components.

The subsurface hypothesis naturally explains the response of the waveguide velocity to groundwater. The waveguide velocity is related to the deep P-wave velocity, and the observed sensitivity to the water-table change, about 0.8×10^{-6} Pa^{-1}, is comparable to the effective pressure sensitivity of the P-wave velocity, about 10^{-6} Pa^{-1} (Yamamura et al., 2003). The positive correlation between the velocity and the water level suggests that the water-table change affects the velocity through loading rather than through pore pressure. The bridge-wave hypothesis naturally explains the rapid diurnal changes, because an exposed structure responds quickly to temperature. The diurnal changes in f_2 and γ_2 can be attributed directly to thermal effects in the structure, and the -0.262% per °C response of f_2 is consistent with the bridge frequency response of about -0.1 to -0.3% per °C (C. Liu & DeWolf, 2007; Zabel et al., 2010). However, the waveguide velocity c_0 associated with the girder shows no clear temperature response, yet correlates

with the groundwater level. It therefore remains to be determined by further observations whether the correlation between the groundwater level and the waveguide velocity is a true coupling, and which path dominates.

Whichever hypothesis holds, the changes we observe are important for monitoring the bridge system. If the wave is carried by the ground, we monitor the foundation of the system; if by the structure, we monitor the girder and its connections. More importantly, in addition to the two conventional monitoring quantities, the structural mode f_2 and the velocity of the medium c_0, we also observe γ_2, a new observable that changes by about 30% over the daily cycle and is highly sensitive to changes in the coupling between components. The seismological method therefore reveals not only changes inside the components but also the coupling at their boundaries, complementing conventional modal monitoring (Hao et al., 2025; Y.-W. Wang et al., 2022; Peeters & De Roeck, 2001) and other vibration-based methods as a joint tool for bridge health.

5 Conclusions

In summary, using a dense array and passing trains as the source, we extracted the dispersion curve of a fast guided wave along the HSR viaduct hour by hour. The dispersion changes in two patterns: a diurnal cycle of up to about 4% at 6.5 Hz that reverses near 7 Hz, and a multi-day change of about 0.6% that is independent of frequency. The diurnal cycle correlates with air temperature, and the multi-day change coincides with the groundwater-level fall caused by irrigation during the observed drawdown. Combining the two patterns with the dispersion features, we proposed a locally resonant model of a waveguide loaded with two subwavelength resonators, which reproduces both the observed dispersion curve and its hourly changes.

Under the model, the diurnal cycle is assigned to changes in the resonance parameters f_2 and γ_2, whereas only a change in the waveguide velocity c_0 can produce a frequency-independent response, so the multi-day change is attributed to c_0. The frequency pattern of the change therefore identifies which part of the viaduct system is changing: the structural mode, the medium that carries the wave, or the coupling between components. Among the fitted parameters, γ_2, the coupling strength, is a quantity that conventional modal monitoring can hardly provide, so the method complements modal and other vibration-based methods. Whichever part of the system carries the wave, the girder or the ground,

this attribution does not depend on the mechanism. In future, we will carry out long-term, multi-region observations across different geological settings, to determine whether the wave is carried mainly by the girder or by the ground, thereby making the attribution of the changes more specific.

Conflict of Interest

The authors declare there are no conflicts of interest for this manuscript.

Acknowledgments

We thank Academician Rixiang Zhu for his support of this high-speed-rail wavefield study, and Geophysical Deep Sensing Technology (GDST), Suzhou, China, for the in-kind support of the instruments used in the observations. We also thank Wang Zhang (Institute of Geology and Geophysics, Chinese Academy of Sciences) for his insights on the writing, and Dr. Yanzhe Zhao and Qiming Zhou (School of Earth and Space Sciences, Peking University) for their participation in the data acquisition. The DeepSeek-V4 language model was used to assist in developing the analysis and plotting code and to polish the language of this manuscript, and all outputs were reviewed and verified by the authors. This study was supported by the National Natural Science Foundation of China (Grant No. 42288201), through the Basic Science Center Program "Craton destruction and terrestrial biological evolution" (Phase II).

Open Research

Data and code supporting this study are openly available in the Zenodo reproduction package (Shi et al., 2026) under a CC BY 4.0 license, which contains the analysis and plotting scripts, the derived data products needed to reproduce every figure, and the groundwater level and meteorological records used here. Supporting information contains Figures S1–S17 and the associated captions.

Author Contributions

Y. Shi: data processing, analysis and visualization, theoretical interpretation, writing. J. Wen: data acquisition, revision. H. Wu: data acquisition, discussion, revision. M. Li: groundwater-level data acquisition and interpretation, discussion. Z. Yu: discussion,

revision. C. He: data acquisition and field funding. L. Chen: project organization, revision. J. Ning: project organization, revision.

References

Bharadwaj, P., Schuster, G., Mallinson, I., & Dai, W. (2012). Theory of supervirtual refraction interferometry: Theory of SVI. *Geophysical Journal International*, *188*(1), 263–273. doi: 10.1111/j.1365-246X.2011.05253.x

Brenguier, F., Boué, P., Ben-Zion, Y., Vernon, F., Johnson, C., Mordret, A., ... Lecocq, T. (2019). Train Traffic as a Powerful Noise Source for Monitoring Active Faults With Seismic Interferometry. *Geophysical Research Letters*, *46*(16), 9529–9536. doi: 10.1029/2019GL083438

Brenguier, F., Courbis, R., Mordret, A., Campman, X., Boué, P., Chmiel, M., ... Hollis, D. (2020). Noise-based ballistic wave passive seismic monitoring. Part 1: Body waves. *Geophysical Journal International*, *221*(1), 683–691. doi: 10.1093/gji/ggz440

Chen, L., & Yan, W. (2022). Achievements and prospects of railway bridge construction technology in China. *High Speed Railway Technology*, *13*(4), 1–7. (In Chinese, with English title) doi: 10.12098/j.issn.1674-8247.2022.04.001

Chen, Z., Lim, C. W., & Shi, F. (2022). A review on seismic metamaterials: From natural toartificial structures. *Chinese Science Bulletin*, *67*(12), 1264–1278. doi: 10.1360/TB-2021-0517

Cheng, F., Xia, J., Wang, B., & Zhang, C. (2025). Unveiling coastal dynamics using telecommunication fiber optic cables. *Science Bulletin*, *70*(12), 1945–1948. doi: 10.1016/j.scib.2025.02.023

Clarke, D., Zaccarelli, L., Shapiro, N. M., & Brenguier, F. (2011). Assessment of resolution and accuracy of the Moving Window Cross Spectral technique for monitoring crustal temporal variations using ambient seismic noise: MWCS: Assessment of resolution and accuracy. *Geophysical Journal International*, *186*(2), 867–882. doi: 10.1111/j.1365-246X.2011.05074.x

Colombi, A., Roux, P., Guenneau, S., Gueguen, P., & Craster, R. V. (2016). Forests as a natural seismic metamaterial: Rayleigh wave bandgaps induced by local resonances. *Scientific Reports*, *6*(1), 19238. doi: 10.1038/srep19238

Fang, N., Xi, D., Xu, J., Ambati, M., Srituravanich, W., Sun, C., & Zhang, X.

(2006). Ultrasonic metamaterials with negative modulus. *Nature Materials*, *5*(6), 452–456. doi: 10.1038/nmat1644

Fu, H., Zhang, H., Xiao, L., Zhan, W., Jiang, J., Chen, Y., & Bian, X. (2026). Stabilizing–sensing synergistic geogrid for high-speed railways. *Nature Communications*, *17*(1), 7397. doi: 10.1038/s41467-026-74260-0

Hao, C., Liu, B., Sun, W., Lu, M., Li, Y., Zhuo, Y., ... Ma, Y. (2025). Review of research and application of health monitoring technology for long-span railway bridges. *Journal of Railway Science and Engineering*, *22*(4), 1662–1685. (In Chinese with English abstract) doi: 10.19713/j.cnki.43-1423/u.T20241122

He, X., Wu, T., Zou, Y., Chen, Y. F., Guo, H., & Yu, Z. (2017). Recent developments of high-speed railway bridges in China. *Structure and Infrastructure Engineering*, *13*(12), 1584–1595. doi: 10.1080/15732479.2017.1304429

Huang, H., Sun, C., & Huang, G. (2009). On the negative effective mass density in acoustic metamaterials. *International Journal of Engineering Science*, *47*(4), 610–617. doi: 10.1016/j.ijengsci.2008.12.007

Jiang, Y., Ning, J., Wen, J., & Shi, Y. (2022). Doppler effect in high-speed rail seismic wavefield and its application. *Science China Earth Sciences*. doi: 10.1007/s11430-021-9843-0

Lamb, H. (1917). On waves in an elastic plate. *Proceedings of the Royal Society of London. Series A*, *93*(648), 114–128. doi: 10.1098/rspa.1917.0008

Liu, C., & DeWolf, J. T. (2007). Effect of temperature on modal variability of a curved concrete bridge under ambient loads. *Journal of Structural Engineering*, *133*(12), 1742–1751. doi: 10.1061/(ASCE)0733-9445(2007)133:12(1742)

Liu, J., Aggarwal, J., Hwang, D., Lee, J., Wu, Y., Yin, F., ... Noh, H. Y. (2025). *Bridge monitoring using existing telecom fiber-optic networks.* Preprint, Research Square. doi: 10.21203/rs.3.rs-7603654/v1

Liu, Y., Yue, Y., Luo, Y., & Li, Y. (2021a). Effects of high-speed train traffic characteristics on seismic interferometry. *Geophysical Journal International*, *227*(1), 16–32. doi: 10.1093/gji/ggab205

Liu, Y., Yue, Y., Luo, Y., & Li, Y. (2021b). The seismic broad-band signature of high-speed trains running on viaducts. *Geophysical Journal International*, *226*(2), 884–892. doi: 10.1093/gji/ggab144

Liu, Z., Zhang, X., Mao, Y., Zhu, Y. Y., Yang, Z., Chan, C. T., & Sheng, P. (2000).

Locally resonant sonic materials. *Science*, *289*(5485), 1734–1736. doi: 10.1126/science.289.5485.1734

Mi, B., & Xia, J. (2023). Extraction of Rayleigh, Love, and Virtual Refraction Waves From 3C High-Speed-Train-Induced Vibrations for Near-Surface Characterization. *IEEE Transactions on Geoscience and Remote Sensing*, *61*, 1–10. doi: 10.1109/TGRS.2023.3318989

Mi, B., & Xia, J. (2026). Estimation of near-surface P-wave velocities from train-traffic-induced guided P-waves. *Geophysics*, *91*(4), KS89-KS97. doi: 10.1190/GEO-2025-0003

Mukherjee, S., Li, Y. E., Stumpf, A., & Zhang, H. (2026). Monitoring Near-Surface Changes Using Anthropogenic Seismic Vibrations. *Geophysical Research Letters*, *53*(6), e2025GL120455. doi: 10.1029/2025GL120455

National Railway Administration. (2026). *2025 railway statistical bulletin.* Retrieved 2026-10-18, from `https://www.nra.gov.cn/xwzx/xwxx/xwlb/202605/t20260529_351348.shtml` (In Chinese)

NOAA National Centers for Environmental Information. (2001). *Global surface hourly [station 54602, Baoding, China; 2024].* NOAA National Centers for Environmental Information. Retrieved 2026-09-15, from `https://www.ncei.noaa.gov/data/global-hourly/`

Peeters, B., & De Roeck, G. (2001). One-year monitoring of the Z24-bridge: Environmental effects versus damage events. *Earthquake Engineering & Structural Dynamics*, *30*(2), 149–171. doi: 10.1002/1096-9845(200102)30:2⟨149::AID-EQE1⟩3.0.CO;2-Z

Schuster, G. T. (2009). *Seismic interferometry.* Cambridge: Cambridge University Press. doi: 10.1017/CBO9780511581557

Shao, J., Wang, Y., & Chen, L. (2022). Near-Surface Characterization Using High-Speed Train Seismic Data Recorded by a Distributed Acoustic Sensing Array. *IEEE Transactions on Geoscience and Remote Sensing*, *60*, 1–11. doi: 10.1109/TGRS.2022.3153831

Sheng, Y., Mordret, A., Sager, K., Brenguier, F., Boué, P., Rousset, B., ... Ben-Zion, Y. (2022). Monitoring Seismic Velocity Changes Across the San Jacinto Fault Using Train-Generated Seismic Tremors. *Geophysical Research Letters*, *49*(19), e2022GL098509. doi: 10.1029/2022GL098509

Shi, Y., Wen, J., & Ning, J. (2022). Theoretical analysis of high-speed rail seismic imaging. *Science China Earth Sciences*. doi: 10.1007/s11430-021-9840-x

Shi, Y., Wen, J., Wu, H., Li, M., Yu, Z., He, C., ... Ning, J. (2026). *Train vibrations reveal internal changes in a high-speed railway viaduct system through dispersion-change patterns of a fast guided wave: Reproduction package (scripts and derived data).* Zenodo. Retrieved from `https://doi.org/10.5281/zenodo.22987561` (Reproduction package, CC BY 4.0) doi: 10.5281/zenodo.22987561

Smith, A., Lott, N., & Vose, R. (2011). The integrated surface database: Recent developments and partnerships. *Bulletin of the American Meteorological Society*, *92*(6), 704–708. doi: 10.1175/2011BAMS3015.1

Wang, G., Song, D., Pang, Z., Wang, F., Dai, H., Li, W., & Wang, B. (2025). Laser interferometry for high-speed railway health inspection using telecom fiber along the line. *Nature Communications*, *16*(1), 4129. doi: 10.1038/s41467-025-59507-6

Wang, X., Chen, W., Wen, J., Ning, J., & Li, J. (2019). The applications of synchrosqueezing time-frequency analysis in high-speed train induced seismic data processing (in Chinese). *Chinese Journal of Geophysics*, *62*(6), 2328–2335. doi: 10.6038/cjg2019M0658

Wang, X., Xia, S., Xiao, C., Luo, J., Chen, W., & Liu, D. (2026). Directional characteristic analysis of wavefields excited by high-speed train seismic sources. *Geophysics*, *91*(4), KS73–KS87. doi: 10.1190/geo-2025-0270

Wang, Y.-W., Ni, Y.-Q., & Wang, S.-M. (2022). Structural health monitoring of railway bridges using innovative sensing technologies and machine learning algorithms: A concise review. *Intelligent Transportation Infrastructure*, *1*, liac009. doi: 10.1093/iti/liac009

Wen, J., Shi, Y., & Ning, J. (2021). Extraction of phase-velocity dispersion curves of high-speed-rail seismic surface waves (in Chinese). *Chinese Journal of Geophysics*, *64*(9), 3246–3256. doi: 10.6038/cjg2021P0252

Yamamura, K., Sano, O., Utada, H., Takei, Y., Nakao, S., & Fukao, Y. (2003). Long-term observation of in situ seismic velocity and attenuation. *Journal of Geophysical Research: Solid Earth*, *108*(B6), 2317. doi: 10.1029/2002JB002005

Yin, C., Shi, Y., Wu, H., Wen, J., & Ning, J. (2024). Theoretical analysis of virtual shot gather generation in the high-speed rail seismic wavefield (in Chinese). *Chinese Journal of Geophysics*, *67*(1), 251–260. doi: 10.6038/cjg2023P0377

Zabel, V., Brehm, M., & Nikulla, S. (2010). The influence of temperature varying material parameters on the dynamic behavior of short span railway bridges. In *Proceedings of the international conference on noise and vibration engineering (isma 2010)* (pp. 1519–1532). Leuven, Belgium.

Zhang, G., Tian, Y., Wang, D., Yan, M., & Wang, J. (2015). Sharp decline and sluggish rise of shallow groundwater level in the central hebei piedmont agricultural region. *Advances in Water Science*, *26*(2), 227–232. (In Chinese with English abstract; hourly water-level monitoring from July 2012 to September 2013 in the central Hebei piedmont, with irrigation-season decline exceeding 1.0 cm/d and non-irrigation rise below 1.0 cm/d) doi: 10.14042/j.cnki.32.1309.2015.02.010

Zhang, Y., Li, Y. E., Zhang, H., & Ku, T. (2019). Near-surface site investigation by seismic interferometry using urban traffic noise in Singapore. *GEOPHYSICS*, *84*(2), B169-B180. doi: 10.1190/geo2017-0798.1